

Theoretical calculation of equilibrium Mg isotope fractionation between silicate melt and its vapor

Haiyang Luo^{1,2} · Huiming Bao^{1,3} · Yuhong Yang⁴ · Yun Liu¹

Received: 24 April 2018 / Revised: 11 June 2018 / Accepted: 5 July 2018 / Published online: 17 July 2018
© Science Press, Institute of Geochemistry, CAS and Springer-Verlag GmbH Germany, part of Springer Nature 2018

Abstract Isotope fractionation during the evaporation of silicate melt and condensation of vapor has been widely used to explain various isotope signals observed in lunar soils, cosmic spherules, calcium–aluminum-rich inclusions, and bulk compositions of planetary materials. During evaporation and condensation, the equilibrium isotope fractionation factor (α) between high-temperature silicate melt and vapor is a fundamental parameter that can constrain the melt’s isotopic compositions. However, equilibrium α is difficult to calibrate experimentally. Here we used Mg as an example and calculated equilibrium Mg isotope fractionation in MgSiO_3 and Mg_2SiO_4 melt–vapor systems based on first-principles molecular dynamics and the high-temperature approximation of the Bigeleisen–Mayer equation. We found that, at 2500 K, $\delta^{25}\text{Mg}$ values in the MgSiO_3 and Mg_2SiO_4 melts were 0.141 ± 0.004 and $0.143 \pm 0.003\text{\textperthousand}$ more positive than in their respective vapors. The corresponding $\delta^{26}\text{Mg}$ values were 0.270 ± 0.008 and $0.274 \pm 0.006\text{\textperthousand}$ more positive than in vapors, respectively. The general $\alpha - T$ equations describing the equilibrium Mg α in MgSiO_3 and Mg_2SiO_4

melt–vapor systems were: $\alpha_{\text{Mg(l)}-\text{Mg(g)}} = 1 + \frac{5.264 \times 10^5}{T^2} \left(\frac{1}{m} - \frac{1}{m'}\right)$ and $\alpha_{\text{Mg(l)}-\text{Mg(g)}} = 1 + \frac{5.340 \times 10^5}{T^2} \left(\frac{1}{m} - \frac{1}{m'}\right)$, respectively, where m is the mass of light isotope ^{24}Mg and m' is the mass of the heavier isotope, ^{25}Mg or ^{26}Mg . These results offer a necessary parameter for mechanistic understanding of Mg isotope fractionation during evaporation and condensation that commonly occurs during the early stages of planetary formation and evolution.

Keywords Equilibrium Mg isotope fractionation · Force constant · Structural optimization · RPFR

1 Introduction

Evaporation and condensation are two of the most common events that occur during the evolution of planetary materials because, according to the nebular hypothesis, all of the materials started as a cloud of molecular vapor and dust, followed by coagulation, impact, and thermal events. Materials evaporate and condense during these processes.

An important fingerprint left behind by evaporation and condensation processes is isotopic compositions of elements. For instance, enrichment of heavy Mg and Si isotopes in Type B calcium–aluminum-rich inclusions (CAIs) can be up to several per mil/amu (Clayton et al. 1988). Several evaporation experiments have been performed under different temperatures, pressures, and compositions of melts to measure Mg and Si isotope fractionation. Significant fractionation was observed only when Type B CAIs were partially molten (Davis et al. 1990; Richter et al. 2002, 2007). To interpret their experimental data, Richter et al. (2002, 2007) proposed a theoretical model based on the Hertz–Knudsen equation and Rayleigh distillation

✉ Haiyang Luo
haiyangluo2014@gmail.com

¹ State Key Laboratory of Ore Deposit Geochemistry, Institute of Geochemistry, Chinese Academy of Sciences, Guiyang 550081, China

² University of Chinese Academy of Sciences, Beijing 100049, China

³ Department of Geology and Geophysics, Louisiana State University, Baton Rouge, LA 70803, USA

⁴ Center for Lunar and Planetary Sciences, Institute of Geochemistry, Chinese Academy of Sciences, Guiyang 550081, China

model. The experimentally observed apparent Mg isotope fractionation factor ($\alpha_{25,24} \approx 0.991$) indicates a much smaller fractionation than the theoretical calculation ($\alpha_{25,24} = \sqrt{23.98504/24.98584} = 0.97977$) (Richter et al. 2007). Recently, Mandybaev et al. (2017) did similar evaporation experiments on CMS-1 precursor material at 1900 °C and also found a large discrepancy, with $\alpha_{25,24} \approx 0.98383$ from their experiment and $\alpha_{25,24} = 0.97980$ from a theoretical calculation.

Several possible explanations have been proposed to account for the discrepancy, including diffusion in the melt, sample size, evaporating species, evaporation coefficient of isotopes, recondensation, and the equilibrium isotope fractionation factor (α). The first three possible causes have been excluded by corresponding experiments and thermodynamic calculations (Richter et al. 2002, 2007), while the last three factors are not well investigated. Among them, equilibrium isotope fractionation is a parameter determined by the ratio of the rate constant of evaporation to that of condensation. Currently, few experiments have been conducted to calibrate equilibrium isotope fractionation between melt and vapor. Two experiments, in which vapor was supposed to be in equilibrium with melt, were done by Richter et al. (2002). They found an equilibrium Mg α_{ik}^{Eq} between CaO–MgO–Al₂O₃–SiO₂ (CMAS) melt and vapor at 1400 °C of $0.99989 \pm 0.00060(2\sigma)$. This calibrated value allows that the fractionation factor could be greater or less than 1.000.

One of the difficulties in getting an accurate experimental result is the design of evaporation experiments at high temperatures, e.g., > 2000 °C. Although α at high temperatures is expected to be small, it should not be ignored. Hin et al. (2017) reported that Earth and differentiated planetary bodies are enriched in ²⁵Mg by 0.02% compared to primitive chondrites, and suggested that equilibrium Mg isotope fractionation between melt and vapor over 2500 K is responsible. This is because predicted potassium isotope fractionation constrained by kinetic Mg isotope fractionation is inconsistent with observed potassium isotope fractionation. In their computation of equilibrium $\alpha_{Mg(l)-Mg(g)}$, the reduced partition function (β) value (Schauble 2011) is based on crystal structure even though crystal structure may not be a good approximation for melt structure when calculating β values, especially at high temperatures.

Equilibrium α between melt and vapor has not been theoretically calculated for Mg or for any other element. Considering that the structure and bond environment of the melt are different from those of the vapor in which an element resides, we expect a small but observable equilibrium isotope fractionation at high temperatures. In this paper, we used Mg as an example to calculate equilibrium

isotope fractionation in MgSiO₃ and Mg₂SiO₄ melt–vapor systems based on first-principles molecular dynamics (FPMD) and high-temperature approximation of the Bigeleisen–Mayer equation. This is a necessary step to understanding evaporation and condensation processes during planetary formation and evolution.

2 Methodology

Simulating the structure of MgSiO₃ and Mg₂SiO₄ melts based on FPMD has proven viable (Stixrude and Karki 2005; de Koker et al. 2008). We first used the Vienna Ab initio Simulation Package (VASP) code (Kresse and Furthmüller 1996) to perform FPMD simulations of the MgSiO₃ and Mg₂SiO₄ melts within the local density approximation (LDA) (Kresse and Hafner 1994) and the generalized gradient approximation (GGA) (Kresse and Joubert 1999). Both ultra-soft pseudopotentials in LDA and the projector-augmented wave method in GGA were used with a cutoff energy of 400 eV and gamma point sampling. A canonical ensemble (e.g. NVT) with periodic boundary conditions was used in the simulation. Our cubic supercells of MgSiO₃ and Mg₂SiO₄ contained 80 atoms (16 formula units) and 112 atoms (16 formula units), respectively. The corresponding volumes were 38.9 and 52.36 cm³/mol. The initial structure was melted at 6000 K and then isochorically quenched to 4000 and 2500 K. We ran FPMD simulation at each temperature for 3 ps. After obtaining the steady structure of the MgSiO₃ and Mg₂SiO₄ melts at 2500 K, we captured snapshots at ionic steps = 2100, 2200, 2300, 2400, 2500, 2600, 2700, 2800, 2900, and 3000. Then, we calculated force constants for each Mg atom in the ten configurations in three situations: all-atom optimization, single-atom optimization, and non-optimization. All-atom optimization means structure optimization is performed for all atoms in the cell, while only the structure of the single atom of interest is optimized in single-atom optimization. Non-optimization means that no structure optimization is conducted. Force convergence criteria EDIFFG in structure optimization is equal to – 0.001. A cutoff energy of 600 eV is used in structure optimization and calculating force constants with EDIFF = 10E–8. The average values of force constants for all Mg atoms in the ten configurations were taken as the approximate force constant for Mg in the melt. Then, we used a high-temperature approximation of the Bigeleisen–Mayer equation (Bigeleisen and Mayer 1947; Wolfsberg et al. 2010) to calculate the reduced partition function ratio (RPFR) of Mg in the melt:

$$\text{RPFR} = 1 + \frac{1}{24} \left(\frac{\hbar}{KT} \right)^2 \frac{1}{4\pi^2} (f_{xx} + f_{yy} + f_{zz})^* \left(\frac{1}{m} - \frac{1}{m'} \right)$$

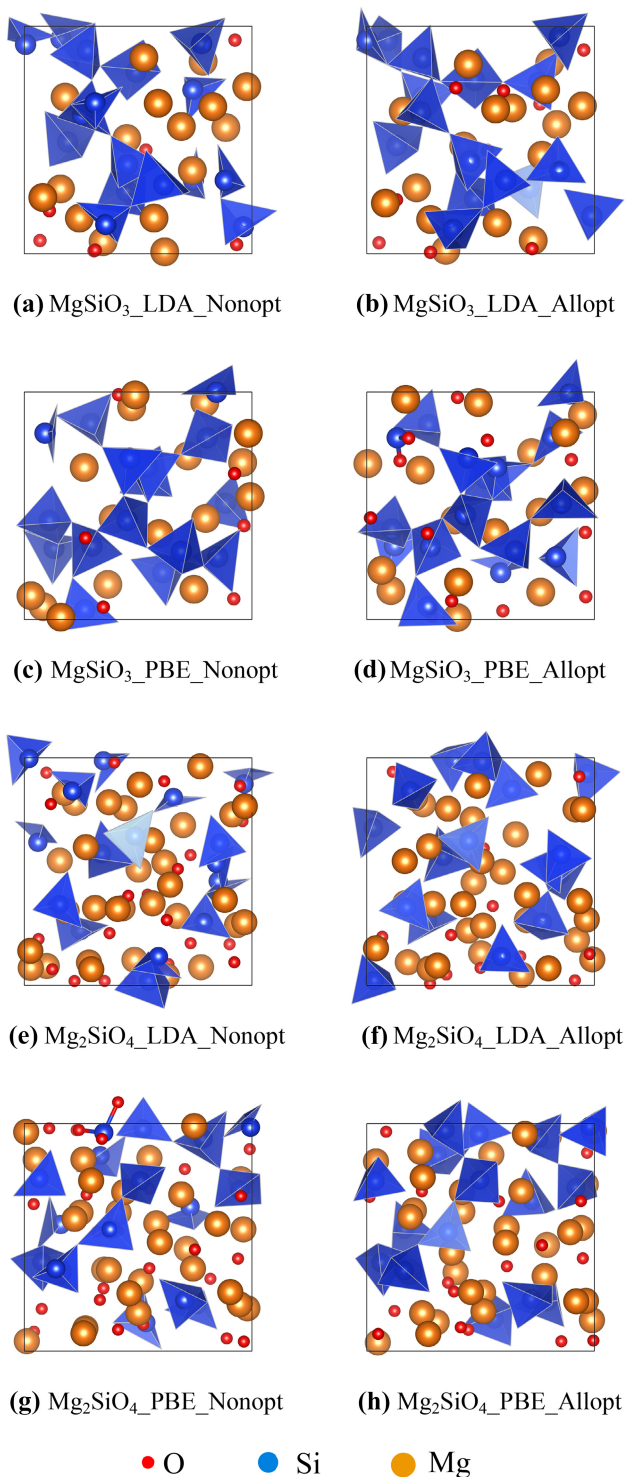


Fig. 1 **a** $\text{MgSiO}_3\text{-LDA}$ is the snapshot of the MgSiO_3 melt at the 2100th step in FPMD within LDA at 2500 K; **b** $\text{MgSiO}_3\text{-LDA_Allopt}$ is the all-atom optimized structure of (a); **c** $\text{MgSiO}_3\text{-PBE}$ is the snapshot of the MgSiO_3 melt at the 2100th step in FPMD within Perdew–Burke–Ernzerhof (PBE) at 2500 K; **d** $\text{MgSiO}_3\text{-PBE_Allopt}$ is the all-atom optimized structure of (c); **e** $\text{Mg}_2\text{SiO}_4\text{-LDA}$ is the snapshot of the Mg_2SiO_4 melt at the 2100th step in FPMD within LDA at 2500 K; **f** $\text{Mg}_2\text{SiO}_4\text{-LDA_Allopt}$ is the all-atom optimized structure of (e); **g** $\text{Mg}_2\text{SiO}_4\text{-PBE}$ is the snapshot of the Mg_2SiO_4 melt at the 2100th step in PBE at 2500 K; **h** $\text{Mg}_2\text{SiO}_4\text{-PBE_Allopt}$ is the all-atom optimized structure of (g)

where f_{xx}, f_{yy} , and f_{zz} are the diagonal elements of the force constant matrix; m the mass of the light isotope; m' the mass of the heavier isotope; T temperature; K the Boltzmann constant; and h Planck's constant.

To calculate equilibrium Mg isotope fractionation between melt and vapor, we also needed the RPFR of Mg in the vapor. One key factor in determining the RPFR of Mg in vapor is the gaseous species of Mg. It has been determined by both experiments and thermodynamic calculations that the dominant gaseous species of Mg over silicate melt is Mg atoms, whose concentration is at least two orders of magnitude higher than the secondary gaseous species, MgO (Richter et al. 2002, 2007). Mg in vapor can be regarded as atomic Mg in form and its RPFR should be 1 given negligible intermolecular bonding in gas. Therefore, the equilibrium $\alpha_{\text{Mg(l)}-\text{Mg(g)}} = \frac{\text{RPFR(l)}}{\text{RPFR(g)}} = \text{RPFR}(l)$.

3 Results

3.1 Structural optimization

We performed all-atom structural optimization based on the extracted configurations to check whether we could obtain metastable structures of the MgSiO_3 and Mg_2SiO_4 melts that represent ideal structures of the melts. As shown in Fig. 1, we used the configuration at ionic step = 2100 as an example and found that all-atom optimized structures maintained the same structural features as non-optimized configurations. One difference was that more silicon–oxygen tetrahedrons were observed in the all-atom optimized structures.

We also analyzed the Si–O and Mg–O radial distribution function (RDF) for the all-atom optimized structure and non-optimized structure of the 2100th configuration. The Si–O and Mg–O RDFs of the melt within the last 1 ps were

used as references. As shown in Fig. 2, the basic shape of the RDFs looks similar, but the first peak for the all-atom optimized structure is much higher than for the non-optimized structure.

3.2 Force constants

We calculated force constants for all Mg atoms in the ten configurations we extracted. Therefore, for MgSiO_3 and Mg_2SiO_4 melts, force constants for 160 and 320 Mg atoms were calculated, respectively. Then, we took the average of the force constants under each condition and computed the corresponding standard errors (Table 1).

As shown, both the force constants and their corresponding standard errors in LDA were smaller than in PBE. Force constants were consistently larger and their corresponding standard errors smaller under all-atom optimization than under single-atom optimization. In addition, the force constant of the Mg_2SiO_4 melt was larger than that of the MgSiO_3 melt under single-atom optimization, but the opposite was the case under all-atom optimization.

3.3 RPFR and fractionation factor

We used the above force constants ($f_{xx} + f_{yy} + f_{zz}$) to calculate the RPFR value of Mg atoms in the MgSiO_3 and Mg_2SiO_4 melts. Table 2 shows the computed results of $1000 \ln \alpha_{25\text{Mg}-24\text{Mg}}$ (%) and $1000 \ln \alpha_{26\text{Mg}-24\text{Mg}}$ (%) and their corresponding standard errors at 2500 K.

A plot of $1000 \ln \alpha_{\text{Mg(l)}-\text{Mg(g)}}$ versus $10^8/T^2$ is shown in Fig. 3.

As we can see, equilibrium Mg isotope fractionation in LDA was smaller than in PBE. Meanwhile, equilibrium Mg isotope fractionation was consistently larger under all-atom optimization than under single-atom optimization.

4 Discussion

Structural comparison and RDF analysis confirmed that ideal metastable structures of the MgSiO_3 and Mg_2SiO_4 melts were obtained after all-atom optimization. More silicon–oxygen tetrahedrons were expected in all-atom optimized structures than in non-optimized structures because atoms in the all-atom optimized structure were in equilibrium positions and distributed more symmetrically. This also explains why RDF for all-atom optimized structures had a much higher peak.

We report two sets of data here. One is based on LDA using ultrasoft pseudopotentials (USPP), the other on GGA using PBE. LDA tends to underestimate computed properties, while GGA tends to overestimate these properties.

Fig. 2 RDFs for MgSiO_3 and Mg_2SiO_4 melts at 2500 K within the last 1 ps (red line), RDFs for the non-optimized structure of the 2100th configuration (black line), and RDFs for the all-atom optimized structure of the 2100th configuration (orange)

Here both isotope fractionation factors and their corresponding standard error in LDA were much smaller than in PBE. The results based on LDA are recommended because FPMD of elasticity, pressure, and volume of silicates has been based on LDA and the results match well with experimental data (Karki 2010). Future experimental data can help validate this recommendation.

The question of which of the three different optimization conditions—non-optimization, single-atom optimization, and all-atom optimization—gives a more accurate equilibrium Mg isotope fractionation factor is determined by a balance between inaccuracy of computation and the deviation from real structures. Although the configurations under the non-optimization condition represented the real structures of a melt, force constants calculated under non-optimized structure were not as credible. The inaccuracy of the computation itself was caused by a failure of harmonic approximation since almost all Mg atoms in the non-optimization situation were not in their equilibrium positions. When the computed force constants for part of the Mg atoms are overlarge, the outcome is an erroneously large isotope fractionation for the non-optimized force constant of the Mg_2SiO_4 melt in PBE. For the metastable structures that we obtained under all-atom optimization, computational inaccuracy was minimized, but the ideal structures may have deviated far from the real melt. The differences in isotope fractionation and the corresponding standard error between all-atom optimization and single-atom optimization were predictable because all-atom optimized structures tend to reach global equilibrium, while single-atom optimization will only reach local equilibrium. Single-atom optimization does not change the position of Si and O atoms around Mg atoms, which means that they inherit part of the non-equilibrium information from the initial snapshot. Thus, it is reasonable to conclude that single-atom optimization closely approximates the real structures and minimizes the computational inaccuracy given those structures.

The values calculated under the single-atom optimized structure in LDA can be regarded as a good estimation of equilibrium Mg isotope fractionation between silicate melt and vapor, whereas the values calculated under the all-atom optimized structure in LDA set the upper limit of equilibrium Mg isotope fractionation in this case. As a result, at 2500 K, $\delta^{25}\text{Mg}$ in MgSiO_3 melt should be more enriched by $0.141 \pm 0.004\%$ compared to Mg atoms in the vapor. And the $\delta^{25}\text{Mg}$ in the Mg_2SiO_4 melt was

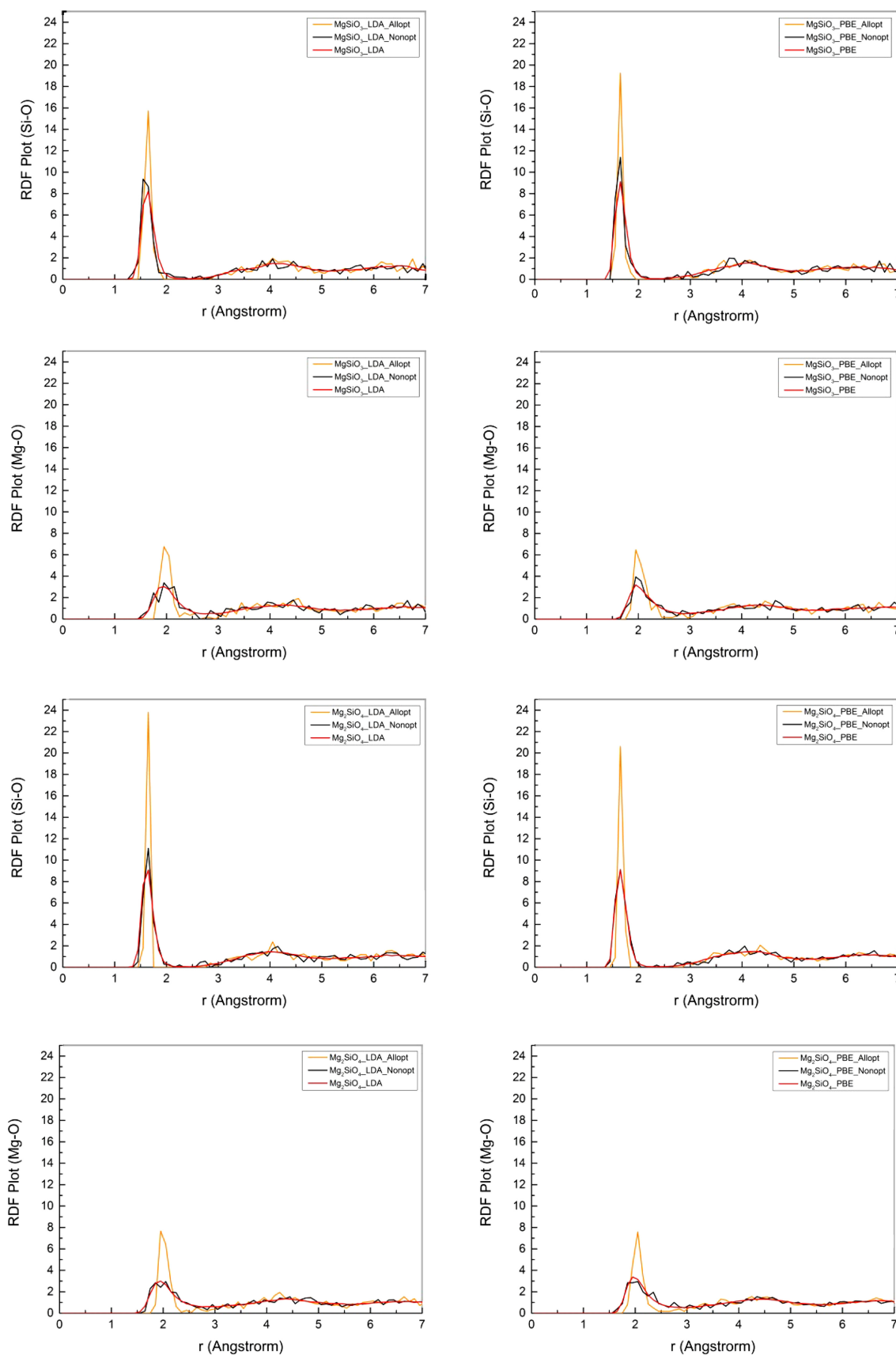


Table 1 Computed force constants under different conditions

MgSiO ₃ melt						
LDA			PBE			
Non-optimization	Single-atom optimization	All-atom optimization	Non-optimization	Single-atom optimization	All-atom optimization	
$f_{xx} + f_{yy} + f_{zz}$	22.911 ± 0.529	22.443 ± 0.654	26.074 ± 0.164	29.466 ± 0.914	27.706 ± 0.736	31.849 ± 0.311
Mg ₂ SiO ₄ melt						
LDA			PBE			
Non-optimization	Single-atom optimization	All-atom optimization	Non-optimization	Single-atom optimization	All-atom optimization	
$f_{xx} + f_{yy} + f_{zz}$	23.303 ± 0.373	22.769 ± 0.458	24.633 ± 0.112	31.888 ± 0.497	29.164 ± 0.780	30.320 ± 0.357

Table 2 Computed $1000 \ln \alpha_{25\text{Mg}-24\text{Mg}}$ (%) and $1000 \ln \alpha_{26\text{Mg}-24\text{Mg}}$ (%) at 2500 K

MgSiO ₃ melt–vapor						
LDA			PBE			
Non-optimization	Single-atom optimization	All-atom optimization	Non-optimization	Single-atom optimization	All-atom optimization	
$1000 \ln \alpha_{25\text{Mg}-24\text{Mg}}$ (%)	0.144 ± 0.003	0.141 ± 0.004	0.163 ± 0.001	0.185 ± 0.006	0.174 ± 0.005	0.200 ± 0.002
$1000 \ln \alpha_{26\text{Mg}-24\text{Mg}}$ (%)	0.276 ± 0.006	0.270 ± 0.008	0.314 ± 0.002	0.354 ± 0.011	0.333 ± 0.009	0.383 ± 0.004
Mg ₂ SiO ₄ melt–vapor						
LDA			PBE			
Non-optimization	Single-atom optimization	All-atom optimization	Non-optimization	Single-atom optimization	All-atom optimization	
$1000 \ln \alpha_{25\text{Mg}-24\text{Mg}}$ (%)	0.146 ± 0.002	0.143 ± 0.003	0.154 ± 0.001	0.200 ± 0.003	0.183 ± 0.005	0.190 ± 0.002
$1000 \ln \alpha_{26\text{Mg}-24\text{Mg}}$ (%)	0.280 ± 0.004	0.274 ± 0.006	0.296 ± 0.001	0.384 ± 0.006	0.351 ± 0.009	0.365 ± 0.004

$0.143 \pm 0.003\%$ higher than that of the gaseous Mg atoms. Meanwhile, calculated $\delta^{26}\text{Mg}$ values in the MgSiO₃ and Mg₂SiO₄ melts were 0.270 ± 0.008 and $0.274 \pm 0.006\%$ heavier than that of vapor Mg, respectively. The general equations we suggest using to obtain the equilibrium Mg α in the MgSiO₃ melt–vapor and Mg₂SiO₄ melt–vapor systems are: $\alpha_{\text{Mg(l)}-\text{Mg(g)}} = 1 + \frac{5.264 \times 10^5}{T^2} (\frac{1}{m} - \frac{1}{m'})$ and $\alpha_{\text{Mg(l)}-\text{Mg(g)}} = 1 + \frac{5.340 \times 10^5}{T^2} (\frac{1}{m} - \frac{1}{m'})$, respectively, where m is the mass of the light isotope and m' the mass of the heavier isotope. As we predicted, we indeed saw small but observable equilibrium Mg isotope fractionation at high temperatures.

According to these general equations, the equilibrium $\alpha_{\text{Mg(g)}-\text{Mg(l)}}^{25} = 0.99969$ at 1400 °C, which lies in the range of experimental data, $\alpha_{ik}^{Eq} = 0.99989 \pm 0.00060(2\sigma)$ (Richter et al. 2002). The causes for deviation may have originated from different melt compositions and approximation of $RPFR(g) = 1$. The latter factor will slightly

overestimate equilibrium isotope fractionation. For different bulk compositions of planetary materials (Hin et al. 2017), the general equation can be used to estimate the loss of initial material provided that the dominant fractionation mechanism for the Rayleigh process is equilibrium melt–vapor isotope fractionation. With this parameter on hand, we are now equipped to calibrate the kinetic isotope effects involving evaporation and condensation so that we can eventually understand Mg isotope behavior during the early stage of planetary formation and evolution.

5 Conclusions

By performing FPMD, calculating force constants based on VASP, and applying the high-temperature approximation of the Bigeleisen–Mayer equation, we obtained equilibrium Mg isotope fractionation between melt and vapor. To get a reliable result, we examined two approximate functions

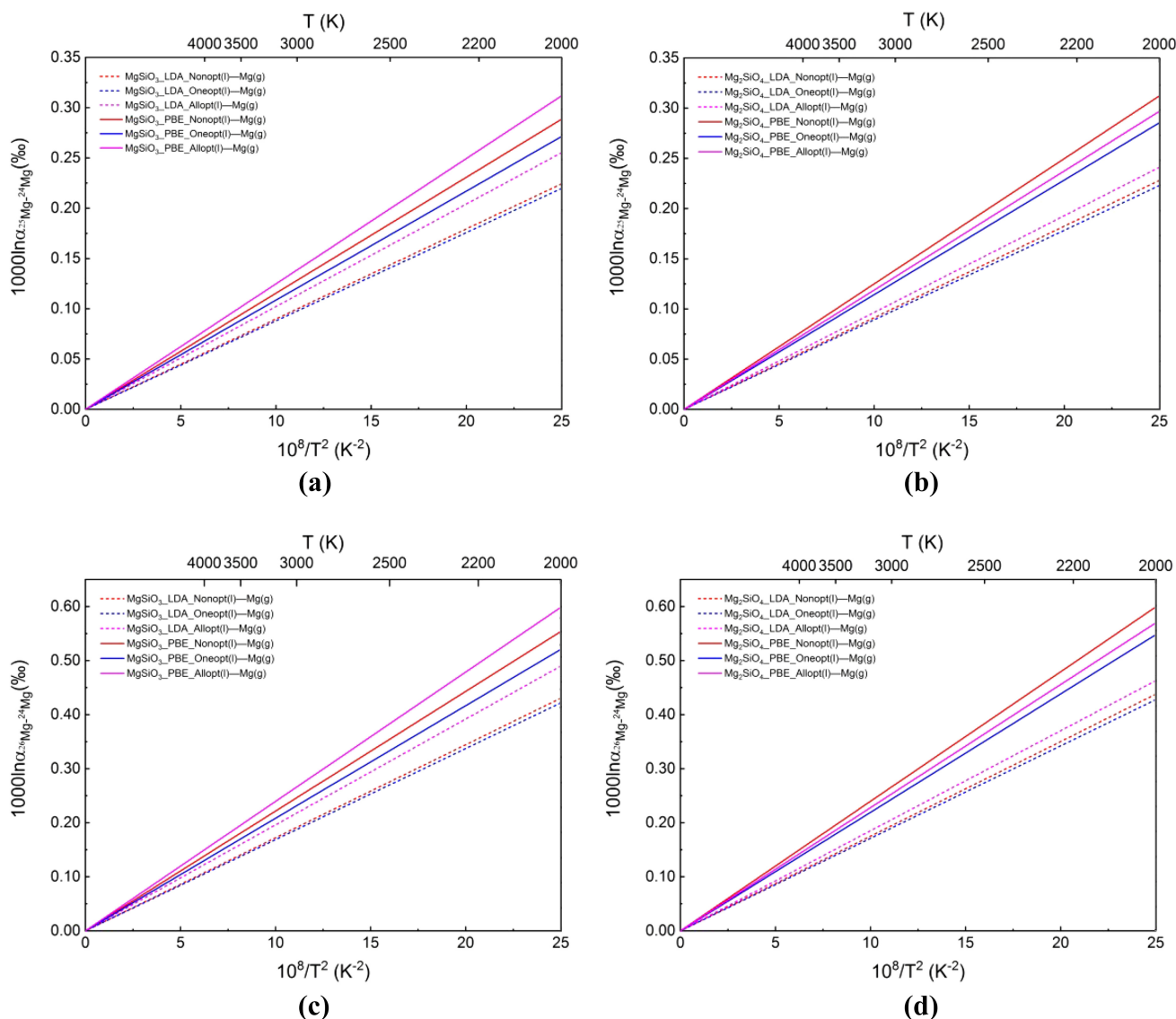


Fig. 3 **a** Computed $1000 \ln \alpha_{25\text{Mg}-24\text{Mg}}$ versus $10^8/T^2$ between the MgSiO_3 melt and gaseous Mg atoms; **b** computed $1000 \ln \alpha_{25\text{Mg}-24\text{Mg}}$ versus $10^8/T^2$ between the Mg_2SiO_4 melt and gaseous Mg atoms; **c** computed $1000 \ln \alpha_{26\text{Mg}-24\text{Mg}}$ versus $10^8/T^2$ between the MgSiO_3 melt and gaseous Mg atoms; **d** computed $1000 \ln \alpha_{26\text{Mg}-24\text{Mg}}$ versus $10^8/T^2$ between the Mg_2SiO_4 melt and gaseous Mg atoms

based on electron density—LDA and GGA; and three structural optimization methods. Equilibrium Mg isotope fractionation based on single-atom optimized structure and LDA was the most reliable. In addition, values based on all-atom optimized structure represent the upper limit of equilibrium Mg isotope fractionation. Our simulation focused on the structure of MgSiO_3 and Mg_2SiO_4 melts only. Multicomponent melts will need more complex computation schemes and are necessary for real-world materials.

Acknowledgements Financial support for this work is provided by the strategic priority research program (B) of CAS (XDB18010104) and China NSFC Grant No. 41490635 to Professor Huiming Bao.

Compliance with ethical standards

Conflict of interest On behalf of all authors, the corresponding author states that there is no conflict of interest.

References

- Bigeleisen J, Mayer MG (1947) Calculation of equilibrium constants for isotopic exchange reactions. *J Chem Phys* 15:261–267. <https://doi.org/10.1063/1.1746492>
- Clayton RN, Hinton RW, Davis AM (1988) Isotopic variations in the rock-forming elements in meteorites. *Philos Trans R Soc A Math Phys Eng Sci* 325:483–501. <https://doi.org/10.1098/rsta.1988.0062>

- Davis AM, Hashimoto A, Clayton RN, Mayeda TK (1990) Isotope mass fractionation during evaporation of Mg_2SiO_4 . *Nature* 347:655. <https://doi.org/10.1038/347655a0>
- de Koker NP, Stixrude L, Karki BB (2008) Thermodynamics, structure, dynamics, and freezing of Mg_2SiO_4 liquid at high pressure. *Geochim Cosmochim Acta* 72:1427–1441. <https://doi.org/10.1016/j.gca.2007.12.019>
- Hin RC et al (2017) Magnesium isotope evidence that accretional vapour loss shapes planetary compositions. *Nature* 549:511. <https://doi.org/10.1038/nature23899>
- Karki BB (2010) First-principles molecular dynamics simulations of silicate melts: structural and dynamical properties. *Rev Mineral Geochem* 71:355–389. <https://doi.org/10.2138/rmg.2010.71.17>
- Kresse G, Furthmüller J (1996) Efficiency of ab initio total energy calculations for metals and semiconductors using a plane-wave basis set. *Comput Mater Sci* 6:15–50. [https://doi.org/10.1016/0927-0256\(96\)00008-0](https://doi.org/10.1016/0927-0256(96)00008-0)
- Kresse G, Hafner J (1994) Norm-conserving and ultrasoft pseudopotentials for first-row and transition elements. *J Phys Condens Matter* 6:8245
- Kresse G, Joubert D (1999) From ultrasoft pseudopotentials to the projector augmented-wave method. *Phys Rev B* 59:1758–1775
- Mendybaev RA, Williams CD, Spicuzza MJ, Richter FM, Valley JW, Fedkin AV, Wadhwa M (2017) Thermal and chemical evolution in the early Solar System as recorded by FUN CAIs: part II—laboratory evaporation of potential CMS-1 precursor material. *Geochim Cosmochim Acta* 201:49–64. <https://doi.org/10.1016/j.gca.2016.08.034>
- Richter FM, Davis AM, Ebel DS, Hashimoto A (2002) Elemental and isotopic fractionation of Type B calcium-, aluminum-rich inclusions: experiments, theoretical considerations, and constraints on their thermal evolution. *Geochim Cosmochim Acta* 66:521–540. [https://doi.org/10.1016/s0016-7037\(01\)00782-7](https://doi.org/10.1016/s0016-7037(01)00782-7)
- Richter FM, Janney PE, Mendybaev RA, Davis AM, Wadhwa M (2007) Elemental and isotopic fractionation of Type B CAI-like liquids by evaporation. *Geochim Cosmochim Acta* 71:5544–5564. <https://doi.org/10.1016/j.gca.2007.09.005>
- Schauble EA (2011) First-principles estimates of equilibrium magnesium isotope fractionation in silicate, oxide, carbonate and hexaaquamagnesium(2+) crystals. *Geochim Cosmochim Acta* 75:844–869. <https://doi.org/10.1016/j.gca.2010.09.044>
- Stixrude L, Karki B (2005) Structure and freezing of $MgSiO_3$ liquid in Earth's lower mantle. *Science* 310:297
- Wolfsberg M, VanHook WA, Paneth P, Rebello LPN (2010) Isotope effects in the chemical, geological, and bio sciences [electronic resource]. Springer, Dordrecht